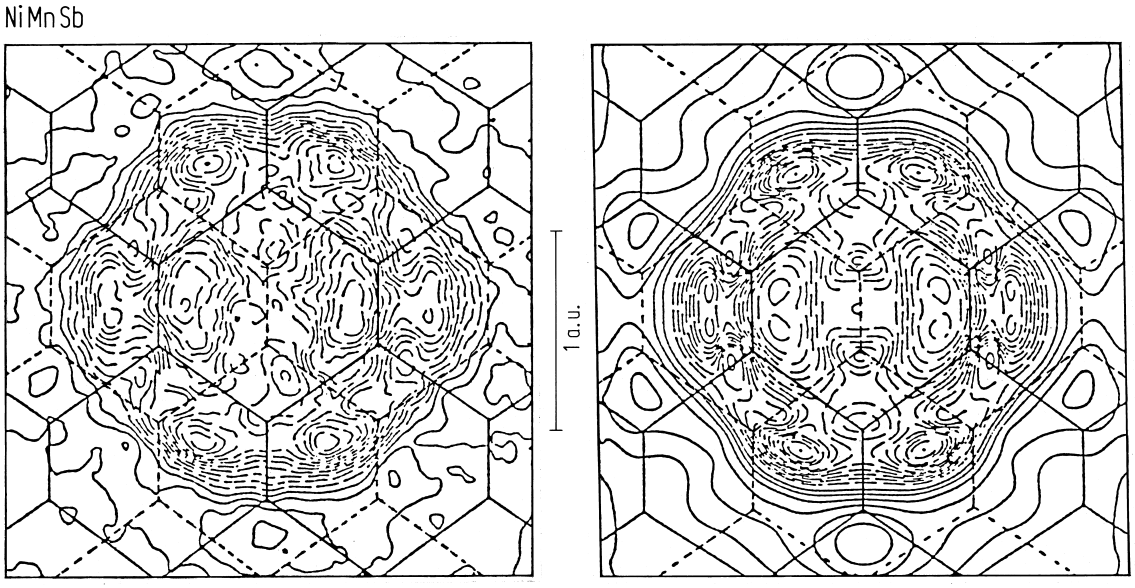

Fig. 595. Difference between the ([110]-integrated) momentum densities of minority and majority spin electrons in NiMnSb, measured with polarised positrons. Left: experiment, right: theory [88M1].

1.5.5.11 Magneto-optics

The response of a medium to electric and magnetic fields is determined by the permittivity and permeability tensors $\boldsymbol{\varepsilon}$ and $\boldsymbol{\mu}$, respectively. For time dependent fields (and in particular for electromagnetic radiation) and for dielectric materials, it is the refractive index n which fully characterises the optical properties. The elements of $\boldsymbol{\varepsilon}$ may be complex and are related to the refractive index by an equation of the form $\boldsymbol{\varepsilon}_{xx} = \left(n_{xx} + \mathrm{i}n'_{xx}\right)^2$. Here $n_{xx}(n'_{xx})$ is the real (imaginary) part of the refractive index n.

For an isotropic material the permittivity is a diagonal tensor. However, if the material is magnetised the macroscopic orientation of the magnetisation singles out a unique direction. As a consequence the permittivity tensor acquires off-diagonal elements which are, to first order, linear in the magnetisation $\boldsymbol{M}$. Thus the permittivity tensor has the form:

$$\boldsymbol{\varepsilon} = \begin{pmatrix} \varepsilon_{xx} & \pm i\varepsilon_{xy} & 0 \\ \mp i\varepsilon_{xy} & \varepsilon_{xx} & 0 \\ 0 & 0 & \varepsilon_{zz} \end{pmatrix}$$

for a magnetisation M which is directed along the z axis ($\boldsymbol{M}||\boldsymbol{z}$). The off-diagonal matrix element is often parameterized in the form

$$Q = \frac{\varepsilon_{xy}}{\varepsilon_{xx}}$$

with Q being the magneto-optic parameter. Q or ε_{xy} change sign if the direction of the magnetisation is reversed. In the literature different sign conventions are in use. For a discussion of the question of the sign convention in magneto-optical calculations and measurements the interested reader is referred to [93A1].

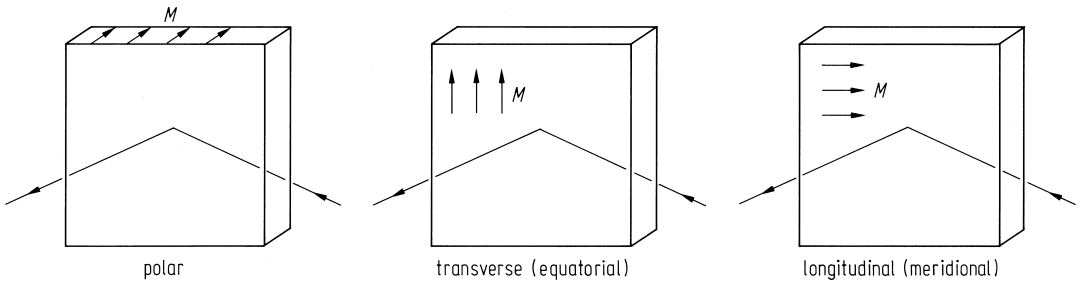

Fig. 596. Experimental arrangements for the orientation of the magnetisation with respect to the surface and the scattering plane (spanned by the incoming and reflected beams) for the polar, longitudinal and transverse Kerr effects.

The off-diagonal element of the permittivity is responsible for the magneto-optical Faraday and Kerr effects. The Faraday effect measures experimentally the rotation of linearly polarised light when passing through a transparent medium and with a magnetic field oriented parallel to the direction of propagation of the light. The Kerr effect is the Faraday measurement carried out on metals and in reflection. For both experiments the polarisation of the incident linearly polarised light is rotated thus acquiring an elliptic component.

Depending on the experimental arrangement the polar, longitudinal and transverse Kerr effect are distinguished. For the polar Kerr effect the magnetisation is oriented perpendicular to the surface of the metal. For the longitudinal and transverse Kerr effects the magnetisation lies in the plane of the surface and is oriented either within or perpendicular to the plane of the incident light.

For the polar Kerr effect consider a cubic material with the conductivity or permittivity tensor $\boldsymbol{\sigma}$ or $\boldsymbol{\varepsilon}$. For the case that the magnetisation is directed along the z axis one obtains the permittivity tensor as

$$\boldsymbol{\varepsilon} = \begin{pmatrix} \varepsilon_{xx} & \mp\varepsilon_{xy} & 0 \\ \pm\varepsilon_{xy} & \varepsilon_{xx} & 0 \\ 0 & 0 & \varepsilon_{zz} \end{pmatrix}$$

The upper signs are applicable if M_z is directed upwards and the lower signs for M_z directed downwards. The off-diagonal elements $\varepsilon_{xy} = \varepsilon_1 - \mathrm{i}\varepsilon_2$ arise due to the spin orbit coupling and give rise to a rotation of the polarisation of the light on reflection. For a non-ferromagnetic sample the random orientation of the magnetisation ensures that the effect cancels out, thus making it observable only for a ferromagnetic sample.

Within a homogeneous medium a plane electromagnetic wave may be described using

$$\begin{pmatrix} \boldsymbol{E}(\boldsymbol{r},t) \\ \boldsymbol{H}(\boldsymbol{r},t) \end{pmatrix} = \begin{pmatrix} \boldsymbol{E}_0 \\ \boldsymbol{H}_0 \end{pmatrix} \cdot \mathrm{e}^{\mathrm{i}\omega\left(t - \frac{n}{c}\boldsymbol{k}\cdot\boldsymbol{r}\right)}$$

This plane wave can be written as a superposition of a wave with a right and a left handed polarisation. The refractive indices for left and right circularly polarised light is then given by

$$n_+ = n(1 + \tfrac{1}{2}Q)$$
$$n_- = n(1 - \tfrac{1}{2}Q)$$

where n is the refractive index without magnetisation. Thus for the polar Kerr effect the experimentally determinable parameters are the phase difference between left and right handed polarised waves and its ellipticity. This yields, respectively, the Kerr rotation angle φ_K and the Kerr ellipticity ε_K. These are related to the magneto-optic parameter Q and the refractive index according to

$$\varphi_K = -\mathrm{Im}\left(\frac{n \cdot Q}{1-n^2}\right) \qquad \varepsilon_K = -\mathrm{Re}\left(\frac{n \cdot Q}{1-n^2}\right)$$

Interest in the magneto-optical properties of $C1_b$ compounds stems from their possible use as thermomagnetic recording media. The stored information can be read by using either the Faraday or the Kerr effect. In both cases sufficiently high signal-to-noise ratios can only be obtained in materials in which these effects are relatively large. The materials must also meet other requirements, e.g., a positive uniaxial anisotropy which can maintain the magnetisation perpendicular to the surface in spite of the demagnetisation field. A further requirement is that the Curie temperature of the compensation point is not too far above room temperature, or the coercive force decreases rapidly with temperature. Measurements have been made on solid surfaces, films and multilayer structures. Particular attention has been focused on PtMnSb, for which a large Kerr effect has been observed. The parameters measured are the Kerr rotation φ_K and Kerr ellipticity ε_K, which are often combined to give an overall Kerr effect Φ_K.

$$\Phi_K = \sqrt{\varphi_K^2 + \varepsilon_K^2}$$

X_2YZ X = 3d, 4d, 5d, Y = 3d

X = 8A: Co, Ni, 1B: Cu
Y = 4A: Ti, Zr, Hf; 7A: Mn
Z = 4B: Sn

X_2YSn

The polar effect has been investigated in cobalt-based Heusler alloys. As Y is changed from Ti to Zr to Hf, the size of the magneto-optical effect increases, which is difficult to understand if the transitions are mainly determined by the Co 3d states. The results for Cu_2MnSn arise predominantly from the exchange split Mn band. For Co_2MnSn the situation is more complicated, since both the Co and Mn atoms carry a moment, but in Ni_2MnSn the moment is confined to the Mn atom.

Table 123. Comparison of the intensity of the main positive peak, *I*, in the magneto-optical spectra of several Co_2YSn compounds with the spin coupling constant γ (taken from Griffith, [61G1]) [83V2].

Y	Ti	Zr	Hf
I [eV^2]	40	250	930
γ [cm^{-1}]	88	339	1336

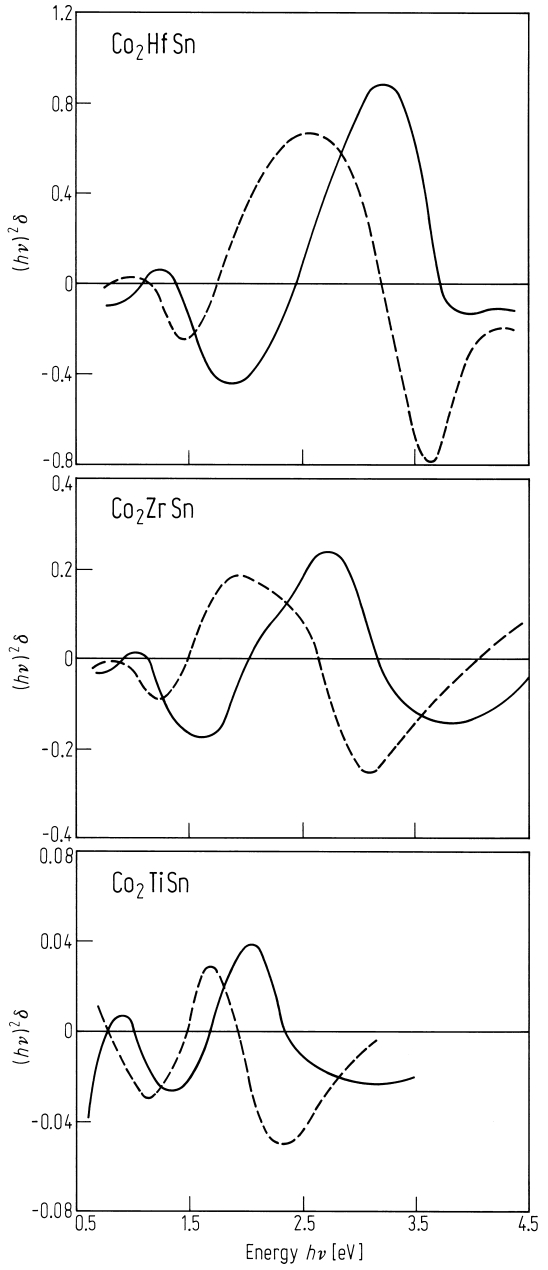

Fig. 597. Comparisons of the energy dependencies of $(h\nu)^2\delta$ in Co_2YSn (Y = Ti, Zr and Hf). δ: off-diagonal element of the dielectric tensor. Solid and broken curves denote the real and imaginary part of the susceptibility, respectively [83V2].

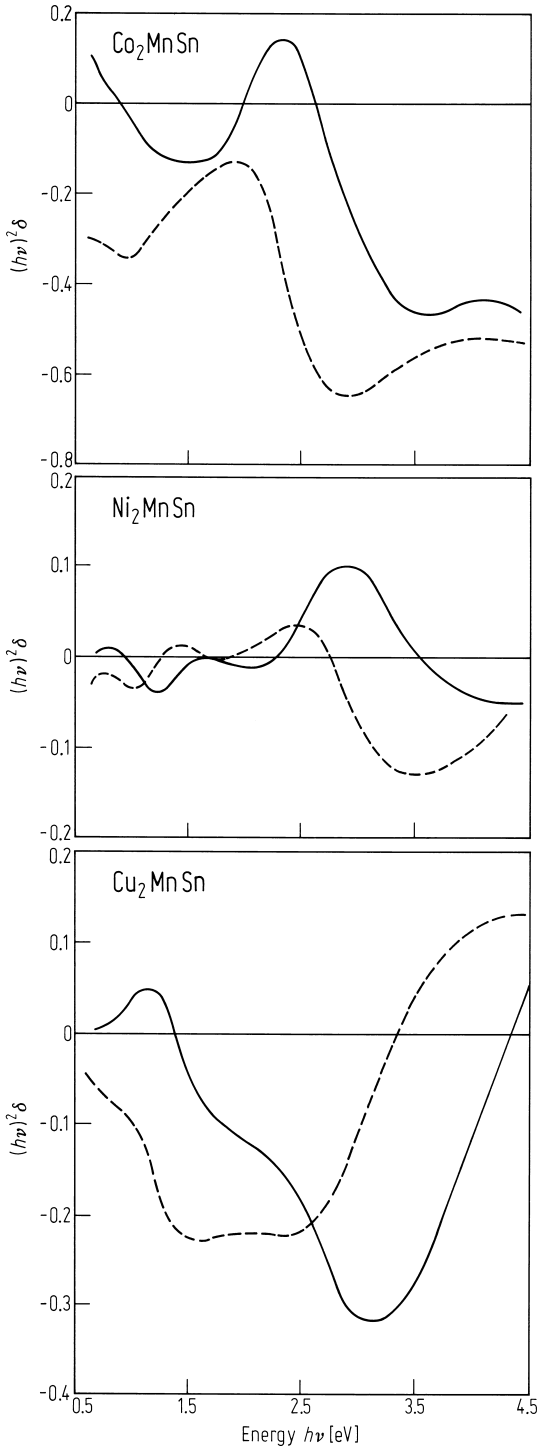

Fig. 598. Energy dependence of $(h\nu)^2\delta$ in X_2MnSn (X = Cu, Ni, Co) [83V2].

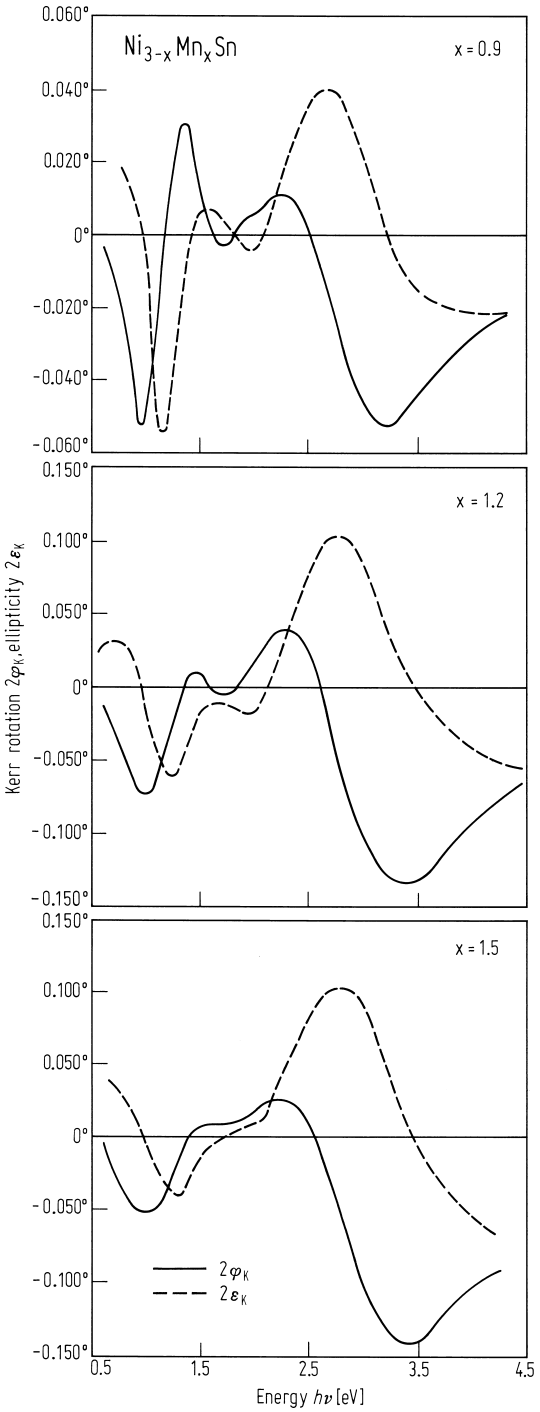

Fig. 599. Energy dependence of the Kerr rotation ($2\varphi_K$; full lines) and the ellipticity ($2\varphi_K$; broken lines) in various Heusler alloys $Ni_{3-x}Mn_xSn$ (x = 0.9, 1.2, 1.5) [84B1].

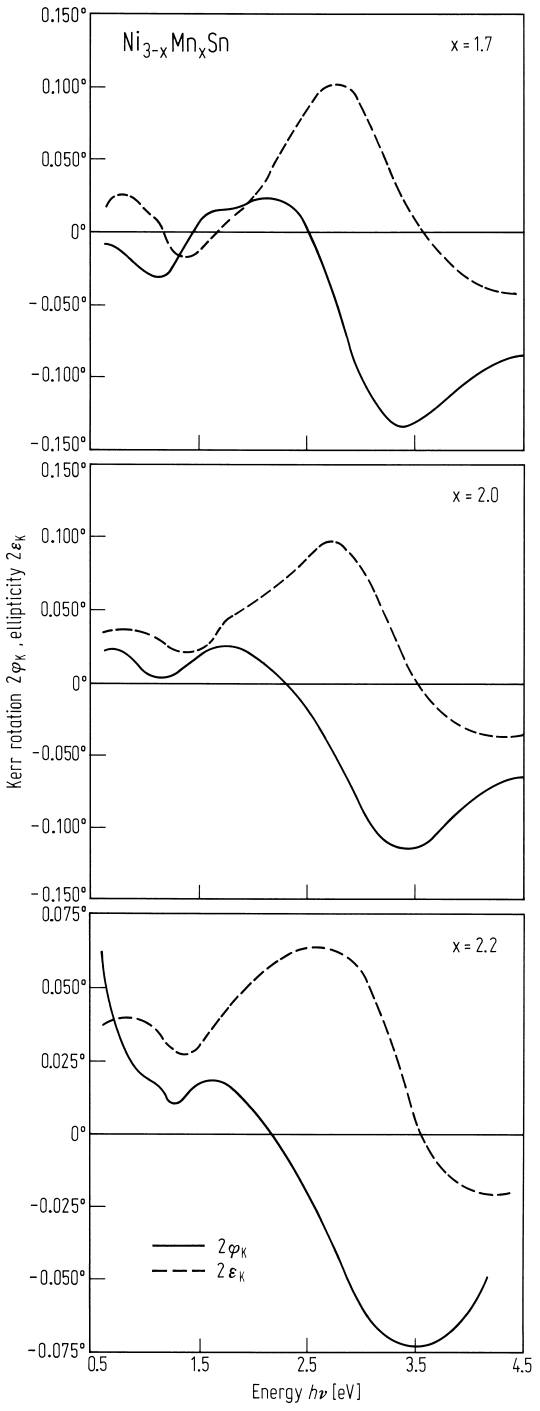

Fig. 600. Energy dependence of the Kerr rotation ($2\varphi_K$; full lines) and the ellipticity ($2\varepsilon_K$; broken lines) in various Heusler alloys $Ni_{3-x}Mn_xSn$ (x = 1.7, 2.0, 2.2) [84B1].

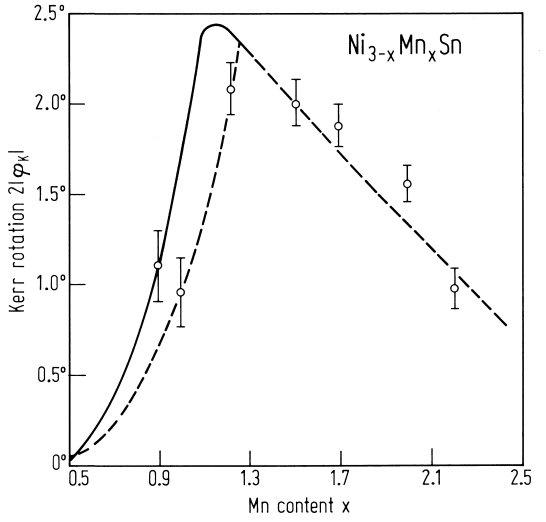

Fig. 601. Concentration dependence of $2\varphi_K$ corresponding to the main peak intensity in the Kerr rotation spectra of the Heusler alloys $Ni_{3-x}Mn_xSn$. In order to exclude effects due to a different temperature dependence of $2\varphi_K$ and in view of the differences in T_C, all $2\varphi_K$ values have been normalised by means of a factor $\sigma(T = 4.2\ K)/\sigma(T = 300\ K)$. The full and broken curves represent the concentration dependence of the main peak intensity as obtained by model calculations of the atomic environment of the nickel atoms [84B1].

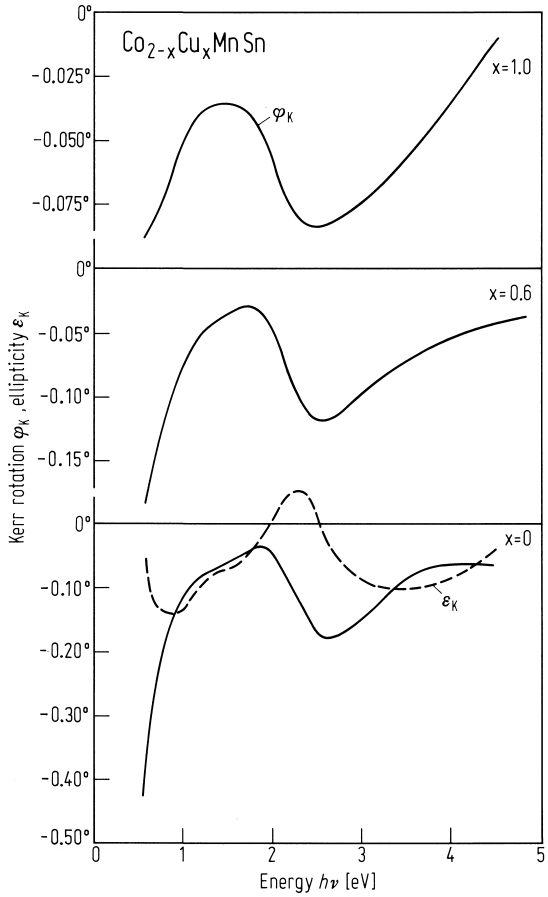

Fig. 603. Kerr rotation φ_K as a function of the energy $h\nu$ in several Heusler compounds of the type $Co_{2-x}Cu_xMnSn$. The ellipticity ε_K is also plotted (broken line) for the compound Co_2MnSn [87V1].

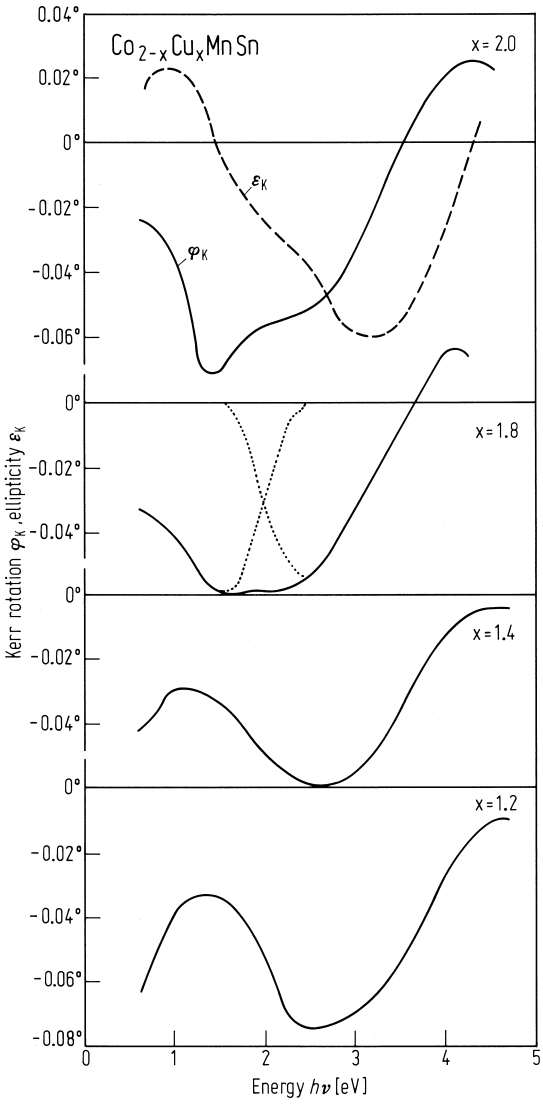

Fig. 602. Kerr rotation φ_K as a function of the energy $h\nu$ in several Heusler compounds of the type $Co_{2-x}Cu_xMnSn$. The ellipticity ε_K is also plotted (broken line) for the compound Co_2MnSn. The dotted line for x = 1.8 indicates the overlaying of two separate closely spaced peaks [87V1].

Summary

Table 124. Crystal chemical, magnetic and magneto-optic data of Fe compounds and alloys. The magnetization σ and polar Kerr rotation angle $2\varphi_K$ were measured at room temperature in an applied field of 1280 kA m^{-1}. $2|\varphi_K|/\sigma$ in 10^{-3}deg kg $A^{-1}m^{-2}$. q: quenched but still multiphased [83B2].

Alloy or compound	Heat treatment	Crystal structure	a [Å]	σ [$Am^2 kg^{-1}$]	$2\varphi_K$ (633 nm)	$2\varphi_K$ (830 nm)	$2\|\varphi_K\|/\sigma$ (633 nm)
Fe	as-cast	bcc (A_2)	2.867	213	– 0.82°	– 1.07°	3.85
$Fe_{90}Al_{10}$	10 d 1000 °C (q)	bcc (A_2)	2.886	203	– 0.83°	– 1.07°	3.1
$Fe_{80}Al_{20}$	10 d 1000 (q)	bcc (A_2)	2.907	185	– 0.78°	– 0.94°	4.2
$Fe_{75}Al_{25}$	10 d 1000 (q)	bcc (A_2)	2.911	162	– 0.79°	– 0.95°	4.9
Fe_3Al	30 d 440	fcc ($D0_3$)	5.805	156	– 0.79°	– 0.96°	5.1
$Fe_{70}Al_{30}$	30 d 600	bcc (A_2)	2.919	98	– 0.69°	– 0.82°	7.8
$Fe_{80}Ga_{20}$	20 d 600	bcc (A_2)	2.907	167	– 0.90°	– 1.12°	5.4
Fe_7Ga_3	30 d 600	fcc ($L1_2$)	3.683	147	– 0.91°	– 1.13°	6.2
$Fe_{70}Ga_{30}$	10 d 900 (q)	bcc (A_2)	2.930	107	– 0.85°	– 1.04°	7.9
Fe_2Ga	6 d 650 (q)	bcc (A_2)	2.917	92	– 0.78°	– 0.90°	8.5
Fe_3Ga_2	18 d 900 (q)	bcc (A_2)	2.89	101	– 0.69°	– 0.88°	6.8
Fe_3Ga_4	90 d 800	monocl.		24	– 0.33°	– 0.38°	13.8
$Fe_{80}Si_{20}$	20 d 900	bcc (A_1)	2.848	160	– 0.73°	– 0.85°	4.6
Fe_3Si	20 d 900	fcc ($L2_1$)	5.662	138	– 0.65°	– 0.72°	4.7

Table 125. Lattice constant a, Curie temperature T_C, saturation moment p_s at 4.2 K, saturation magnetisation σ at 300 K, and Kerr rotation $2\varphi_K$ measured in various Heusler alloys [83B2]. $2|\varphi_K|/\sigma$ in 10^{-3}deg kg $A^{-1}m^{-2}$.

Alloy or compound	Heat treatment	a [Å]	T_C [K]	p_s [μ_B/f.u.]	σ [$Am^2 kg^{-1}$]	$2\varphi_K$ (633 nm)	$2\varphi_K$ (830 nm)	$2\|\varphi_K\|/\sigma$ (633 nm)
Mn_2VAl	30 d 800	5.897		1.82	50	0.02°	0.01°	0.4
Fe_2NiAl	30 d 600	5.758		4.25	117	– 0.50°	– 0.61°	4.3
Fe_2MnAl	12 d 900	5.816		1.58	52	– 0.25°	– 0.28°	4.8
Fe_2CrAl	11 d 800	5.805	246	1.67		– 0.22°	– 0.24°	
Fe_2VAl	11 d 800	5.761	$\chi_g = 1.8 \cdot 10^{-5}$ cm^3 g^{-1}					
Fe_2TiAl	14 d 900	5.879	123	0.11				
Fe_2MoAl	as-cast	5.918		0.36				
Co_2FeAl	10 d 800	5.730		4.96	138	– 0.74°	– 0.84°	5.4
Co_2MnAl	as-cast	5.749	693	4.04	104	– 0.09°	– 0.08°	0.9
Co_2CrAl	as-cast	5.727	334	1.55	17	– 0.02°	– 0.02°	1.2
Co_2VAl	as-cast	5.772	310	1.95	27	– 0.03°	– 0.03°	1.1
Co_2TiAl	14 d 800	5.847	134	0.74				
Co_2NbAl	10 d 900	5.935	383	1.35	22	– 0.01°	– 0.01°	0.5
Co_2ZrAl	3 d 1050	6.078	178	0.79				
Co_2TaAl	10 d 900	5.930	260	1.50				
Co_2HfAl	3 d 1000	6.045	193	0.82				
Ni_2MnAl	8 d 900	5.824	$T_N = 30$					
Ni_2CrAl	as-cast	5.737	140	0.13		– 0.02°	– 0.02°	
Cu_2MnAl	10 d 800	5.968	603	3.60	86			

Table 126. Lattice constant a, Curie temperature T_C, saturation moment p_s at 4.2 K, saturation magnetisation σ at 300 K, and Kerr rotation $2\varphi_K$ measured in various Heusler alloys of the type X_2YGa [83B2]. $2|\varphi_K|/\sigma$ in 10^{-3}deg kg $A^{-1}m^{-2}$.

Compound	Heat treatment	a [Å]	T_C [K]	p_s [μ_B/f.u.]	σ [$Am^2 kg^{-1}$]	$2\varphi_K$ (633 nm)	$2\varphi_K$ (830 nm)	$2\|\varphi_K\|/\sigma$ (633 nm)
Mn_2VGa	as-cast	6.095		1.66	44.3	0	0	0
Fe_2NiGa	2w 800	5.780		3.21	55.0	– 0.31°	– 0.30°	5.6
Fe_2CoGa	10 d 800	5.767		5.09	120.9	– 0.83°	– 0.95°	6.9
Fe_2CrGa	11 d 800	5.824		2.60	42.5	– 0.36°	– 0.41°	8.5
Fe_2VGa	11 d 800	5.782	$\chi_g = 3\cdot10^{-6}$ cm^3 g^{-1}					
Co_2FeGa	10 d 800	5.737		5.13	116.8	– 0.82°	– 0.98°	7.0
Co_2MnGa	10 d 800	5.767	694	4.05	87.5	– 0.28°	– 0.31°	3.2
Co_2CrGa	30 d 800	5.805		2.36	49.3	0	0	0
Co_2VGa	30 d 800	5.779	352	1.92	33.2	– 0.04°	– 0.03°	1.2
Co_2NbGa	14 d 800	5.950		1.39	20.9	– 0.02°	– 0.02°	1.0
Co_2TiGa	as-cast	5.850	130	0.75				
Co_2HfGa	as-cast	6.032	186	0.60				
Ni_2MnGa	8 d 900	5.835	379	4.07	69.7	0	0	0

Table 127. Crystal chemical, magnetic and magneto-optical data of Heusler ($L2_1$-type) compounds based on Sn. The saturation magnetisation per formula unit, p_s, was derived from magnetisation measurements at 4.2 K in a field of 1440 kA/m. The magnetisation σ and the polar Kerr rotation angle $2\varphi_K$ were obtained at room temperature in a field of 1280 kA/m [83B2].
$2|\varphi_K|/\sigma$ in 10^{-3}deg kg $A^{-1}m^{-2}$.

Compound	Heat treatment	a [Å]	T_C [K]	p_s [μ_B/f.u.]	σ [$Am^2 kg^{-1}$]	$2\varphi_K$ (633 nm)	$2\varphi_K$ (830 nm)	$2\|\varphi_K\|/\sigma$ (633 nm)
Fe_2VSn	50 d 600	5.959	200	1.32	8	– 0.05°	0.07°	0.1
Co_2TiSn	30 d 800	6.076	371	1.96	35.8	0	0.01°	0
Co_2ZrSn	20 h 900	6.242	448	1.46		0.18°	– 0.04°	
Co_2HfSn	11 d 800	6.227	394	1.57	19.8	0.31°	0	15.7
Co_2VSn	14 d 800	5.960	95	1.21		0.02°	0.01°	
Co_2NbSn	60 d 600	6.142	105	0.69				
Co_2MnSn	10 d 800	5.984	829	4.79	87.3	– 0.06°	– 0.11°	0.7
Ni_2MnSn	30 d 800	6.048	345	4.01	48	0.01°	0.02°	0
Cu_2MnSn	20 d 640	6.168	530	3.97	60.8	– 0.12°	– 0.14°	2.0

Table 128. Crystal chemical, magnetic and magneto-optical properties of several Heusler ($L2_1$-type) compounds based on Si, Ge, In, Sn and Pb. The saturation magnetisation per formula unit, p_s, was obtained from magnetic measurements at 4.2 K in a field of 18 kOe. The values of the magnetisation σ and the polar Kerr rotation angle $2\varphi_K$ were obtained at room temperature in a field of 1280 kA/m (16 kOe) [83B2].
$2|\varphi_K|/\sigma$ in 10^{-3}deg kg $A^{-1}m^{-2}$.

Compound	Heat treatment	a [Å]	T_C [K]	p_s [μ_B/f.u.]	σ [$Am^2 kg^{-1}$]	$2\varphi_K$ (633 nm)	$2\varphi_K$ (830 nm)	$2\|\varphi_K\|/\sigma$ (633 nm)
Co_2FeSi	20 d 600	5.647	980	5.18	139.8	– 0.67°	– 0.68°	4.8
Fe_2VSi	11 d 800	5.675		$\chi_g = 2.5 \cdot 10^{-5}$ $cm^3 g^{-1}$				
Co_2TiSi	12 d 900	5.743	375	1.65	37.3	0	– 0.05°	0
Fe_2MnSi	10 d 800	5.671		2.33		– 0.05°	– 0.04°	
Co_2MnSi	30 d 800	5.645	985	4.90	138.4	0	– 0.06°	0
Co_2FeGe	20 d 600	5.738		5.54	124.2	– 0.87	– 1.03°	7.0
Co_2MnGe	10 d 800	5.749	905	4.93	108.8	– 0.03°	– 0.08°	0.3
Co_2TiGe		5.807	386	1.59	26.6	0.01°	– 0.01°	0.4
Fe_2CoGe	14 d 800	5.775			118.2	– 0.71°	– 0.79°	6.0
Ni_2MnIn	20 d 600	6.075	323	4.34	40.3	0	0	0
Cu_2MnIn	20 d 520	6.206	500	3.95	64.1	– 0.05°	– 0.03°	0.8
Co_2FeIn	30 d 400	5.716				– 0.88°	– 1.17°	
Rh_2MnSn	24 d 800	6.232	410	3.4	41	0.01°	0.02°	0.2
Rh_2MnGe	as-cast	6.044			27	0	0.01°	0
Rh_2MnPb	as-cast	6.271	335	2.9	3.5	0	0	0
Ru_2FeSn	24 d 800	6.202			33	– 0.14°	– 0.08°	4.2

$C1_b$ XYZ X = 3d, 4d Y = 3d

X = 8A: Ni, Pd, Pt
Y = 7A: Mn; 8A: Fe
Z = 4B: Sn, 5B: Sb

The magneto-optical properties of these compounds have been studied on solid film and multilayer structures. The effects of composition, heat treatment and surface quality on the magneto-optical properties have been investigated.

Solid

Table 129. Crystallographic and magnetic properties of some Mn-based Heusler alloys [83V1].

Compound	a [Å]	p_s [μ_B/Mn]	T_C [K]
PtMnSb	6.210	3.97	582
PdMnSb	6.285	3.95	500
NiMnSb	5.920	3.85	730
PtMnSn	6.264	3.42	330

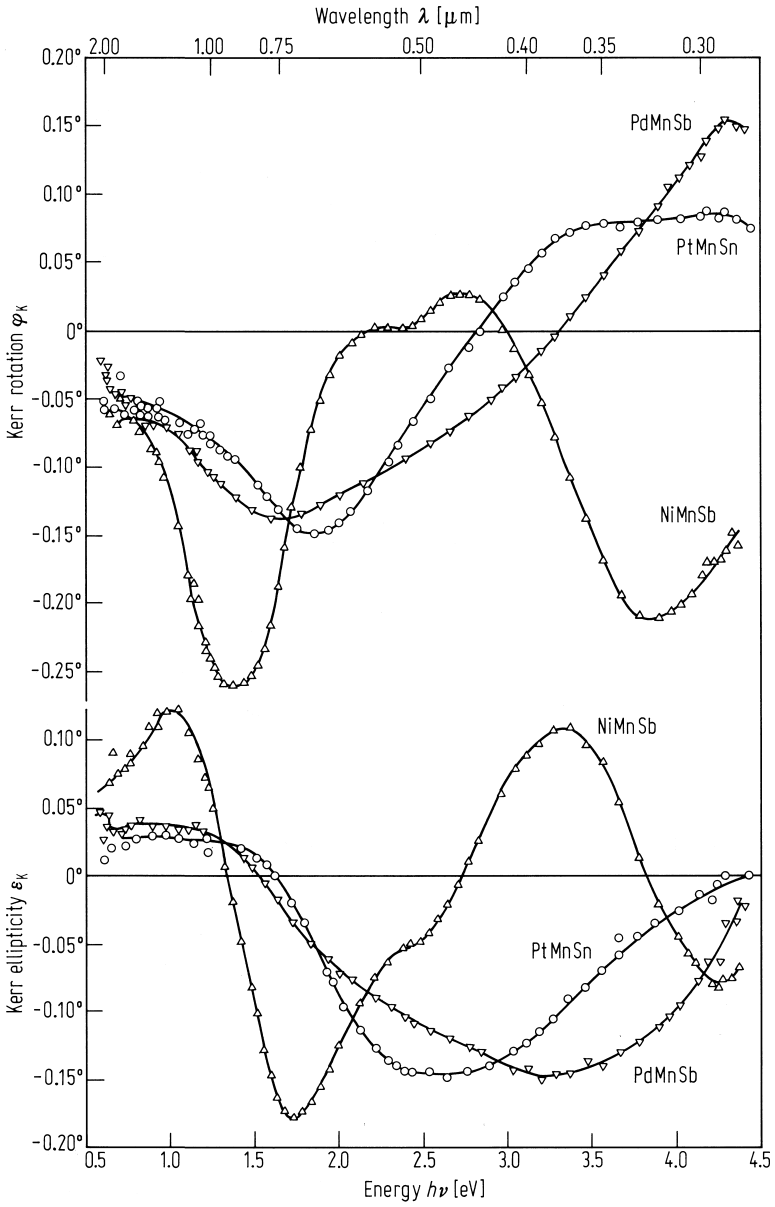

Fig. 604. Kerr rotation (upper part) and Kerr ellipticity (lower part) of PdMnSb, NiMnSb and PtMnSn vs. photon energy [83V1].

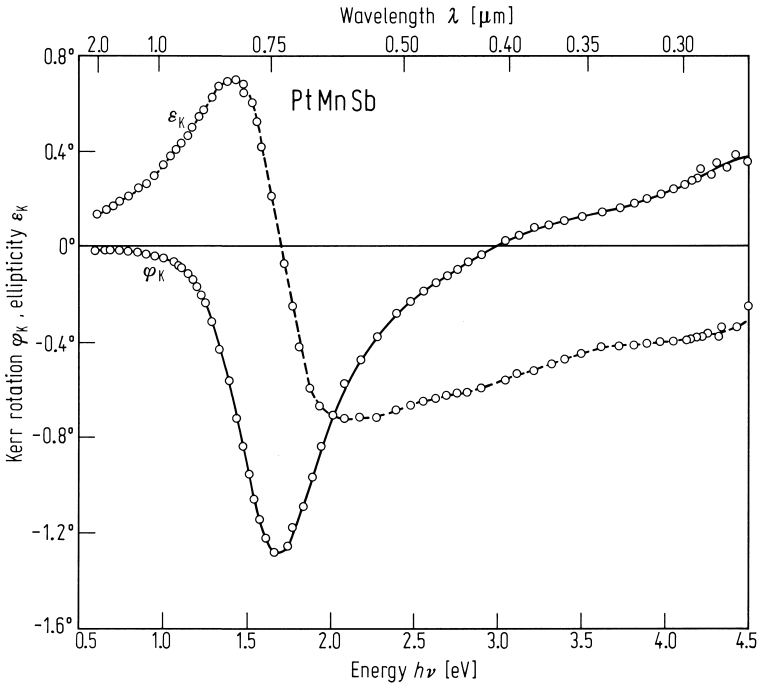

Fig. 605. Kerr rotation and Kerr ellipticity of PtMnSb vs. photon energy [83V1].

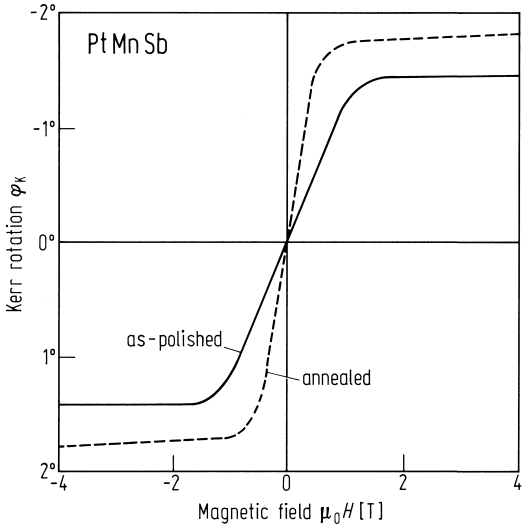

Fig. 606. Magnetic field dependence of the Kerr rotation angle φ_K at 632.8 nm for bulk samples of PtMnSb. Solid line: as-polished sample; dashed line: sample polished and then annealed at 500 °C [90T2].

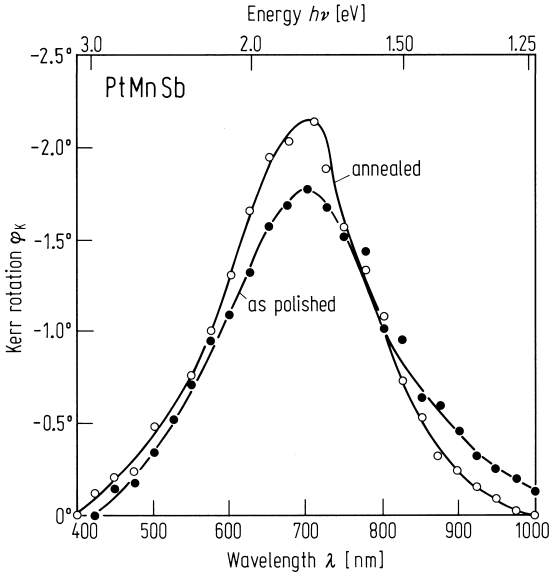

Fig. 607. Spectra of the Kerr rotation angle φ_K for PtMnSb samples. Solid circles: as-polished sample; open circles: sample polished and then annealed at 500 °C [90T2].

Table 130. Compositional dependence of the magnetic and magneto-optical properties of PtMnSb alloys [90T2]. w: weak, vw: very weak.

Sample	Composition [at%]			Structure type	σ [G cm^3 g^{-1}]	$2\varphi_K$
	Pt	Mn	Sb			
1	33.5	33.4	33.1	$C1_b$	54.3	1.75°
2	32.2	35.1	32.7	$C1_b$	52.3	1.34°
3	31.9	37.2	30.9	$C1_b$	50.5	0.73°
4	29.9	40.2	29.9	$C1_b$	47.5	0.64°
5	34.4	31.8	33.8	$C1_b$ + C2 (w)	46.0	1.38°
6	36.0	30.2	33.8	$C1_b$ + C2 (w) + $L1_0$ (w)	37.5	1.07°
7	37.5	31.1	31.4	$C1_b$ + C2 (w) + $L1_0$ (w)	28.7	0.78°
8	30.2	35.1	34.7	$C1_b$ + C2 (vw) + $B8_1$ (w) + $L1_0$ (vw)	51.6	1.39°
9	32.0	31.6	36.4	$C1_b$ + C2 (w)	49.5	0.82
10	35.3	34.7	30.0	$C1_b$ + $L1_0$ (w)	44.8	1.48°

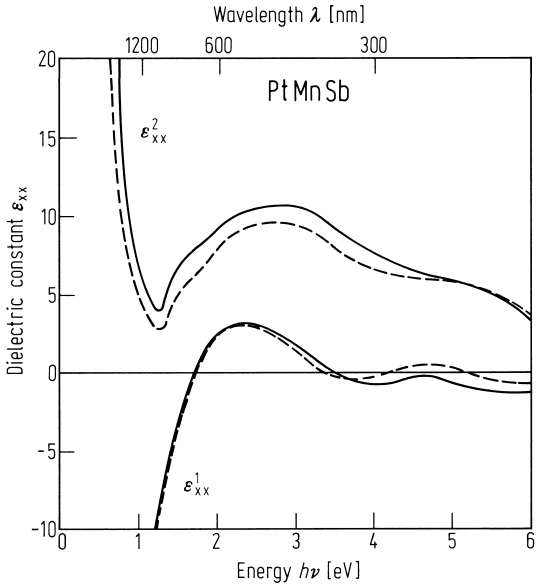

Fig. 608. Real (ε^1_{xx}) and imaginary (ε^2_{xx}) parts of the diagonal elements of the dielectric constant tensor for PtMnSb samples. Solid line: as-polished sample; dashed line: sample polished and then annealed at 500 °C [90T2].

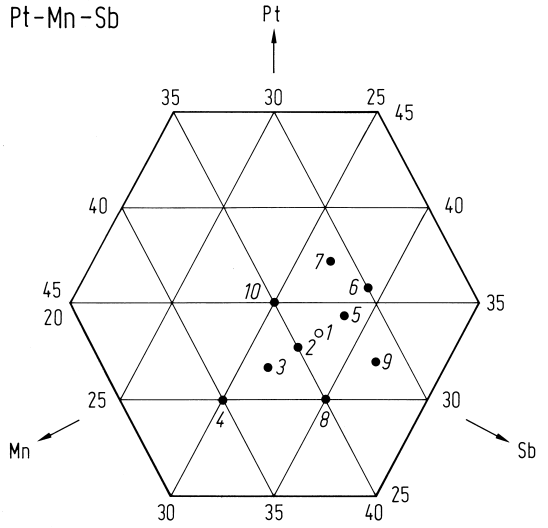

Fig. 609. Composition of ten PtMnSb ternary samples as given in Table 130. Sample 1 represents the stoichiometric composition [90T2]. Numbers of the samples correspond to those in the table.